Band hybridization and spin-splitting in InAs/AlSb/GaSb type II and broken-gap quantum wells

W. Xu,[1,2,a)] L. L. Li,[1] H. M. Dong,[1] G. Gumbs,[3] and P. A. Folkes[4]
[1]*Key Laboratory of Materials Physics, Institute of Solid State Physics, Chinese Academy of Sciences, Hefei 230031, China*
[2]*Department of Physics, Yunnan University, Kunming 650091, China*
[3]*Hunter College, City University of New York, New York 10021, USA*
[4]*U.S. Army Research Laboratory, Adelphi, Maryland 20783, USA*

(Received 27 April 2010; accepted 12 July 2010; published online 8 September 2010)

We present a detailed theoretical study on the features of band hybridization and zero-field spin-splitting in InAs/AlSb/GaSb quantum wells (QWs). An eight-band $\mathbf{k}\cdot\mathbf{p}$ approach is developed to calculate the electronic subband structure in such structures. In the absence of the AlSb layer, the hybridized energy gaps can be observed at the anticrossing points between the lowest electron subband and the highest heavy-hole subband in the InAs and GaSb layers respectively. In such a case, the position and magnitude of the gaps are spin-dependent. When a thin AlSb layer is inserted between the InAs and GaSb layers, we find that the lowest electron subband in the InAs layer is only hybridized with the highest light-hole subband which is also hybridized with the highest heavy-hole subband in the GaSb layer. The hybridized energy gaps and spin-splitting in the InAs/AlSb/GaSb QWs are reduced significantly. These results can be used to understand why electrons and holes can be well separated and why relatively high mobilities for electrons and holes can be achieved in InAs/AlSb/GaSb type II and broken-gap QWs. The present study is relevant to the applications of InAs/GaSb based QW structures as new generation of high-density and high-mobility electronic devices. © *2010 American Institute of Physics*. [doi:10.1063/1.3476059]

I. INTRODUCTION

In type II and broken-gap heterostructures such as InAs/GaSb based quantum wells (QWs), the bottom of the conduction subband in the InAs layer is significantly lower than the top of the valence subband in the GaSb layer.[1,2] In such case both electrons and holes can be conducting and they are spatially separated, respectively, in the InAs and GaSb layers so that the electrons and holes coexist in the structure. The main advantage of an InAs/GaSb type II and broken-gap QW is that once the structure is formed, a single Fermi level is established in the electron-hole bilayer system and high carrier density can be achieved. Because the intentional doping (such as the modulation doping and background doping) is unnecessarily required, the relatively high carrier mobility can also be achieved in the InAs/GaSb type II and broken-gap QWs duo to the absence of the impurity scattering induced by the ionized dopants. On the basis of these unique and important features, InAs/GaSb based QWs have been considered as natural candidates for advanced electronic and optoelectronic devices including negative persistent photoconductors,[3] intrinsic excitonic devices,[4] infrared lasers,[5] interband tunneling devices,[6] uncooled mid-infrared photodetectors,[7] to mention but a few. It is found both experimentally[8] and theoretically[9] that in InAs/GaSb based type II and broken-gap QWs, the dispersion relations for electron and hole subbands along the two-dimensional (2D)-plane (the plane perpendicular to the growth direction) are hybridized and mixed due to the coupling of the conduction band (CB) and valence band in different material layers. As a result, the anticrossing phenomenon can occur at a finite value of the 2D-wavevector $\mathbf{k}_{\|}$ for carriers. The so-produced small hybridization gap (~10 meV) in the dispersion relations has been observed experimentally and confirmed theoretically.[8] In particular, the experimental and theoretical work[8] has demonstrated that this hybridization gap is responsible for the giant negative magnetoresistance in InAs/GaSb based type II and broken-gap heterostructures.

Over the last two decades, the intensive theoretical studies have been undertaken in investigating the electronic subband structures of InAs/GaSb based type II and broken-gap heterostructures using techniques such as the $\mathbf{k}\cdot\mathbf{p}$ method on the basis of Burt's Hamiltonian,[9] the pseudopotential plane-wave approach[10] and the effective bond orbit model.[11] In addition to these methods, it was proposed theoretically that the tunnel interaction in an InAs/GaSb QW can also be used in the calculation of the electronic subband structure.[12] The results obtained from these calculations have shown generally the interesting and important features of the hybridization of the conduction subbands in the InAs layer and the valence subbands in the GaSb layer in InAs/GaSb QW systems.[9–12] Furthermore, it should be noted that in an InAs/GaSb type II and broken-gap QW, due to the presence of the kinetic interactions between the conduction and valence subbands in different material layers, the strong zero-field spin-splitting can be observed. In such case, the spin-orbit interaction is resulted from the bulk inversion asymmetry which

a)Author to whom correspondence should be addressed. Electronic mail: wenxu_issp@yahoo.cn.

is enhanced significantly because of the presence of the asymmetric potential well structures in the InAs/GaSb layers.[9,12]

As is well known, a large carrier density and a high carrier mobility are the two most important sample parameters in the designing of practical electronic devices such as high-electron-mobility transistors (HEMTs) and high speed field-effect transistors (HSFETs). In the conventional InAs/GaSb type II and broken-gap QW structures, the electron-hole hybridization or coupling can lead to a reduction in the electron/hole densities and mobilities. The previous theoretical work[9] has found that the hybridization gap between the electronlike states and the heavy-hole (HH)-like states decreases rapidly with increasing the InAs layer thickness and/or decreasing the GaSb layer widths. For example, by taking the well widths $L_{\mathrm{InAs}} \geq 15$ nm and $L_{\mathrm{GaSb}}=10$ nm the hybridization gap and the spin-splitting can be significantly reduced.[9] Thus, to grow InAs/GaSb QW structures with relatively wide InAs layer width and narrow GaSb layer thickness is a practical way to avoid strong band hybridization in the electronic devices. On the basis that the band hybridization in an InAs/GaSb QW is mainly induced by the kinetic interactions between the conduction subbands and valence subbands in different material layers, the hybridization effect can also be reduced if the penetration of the electron and hole wave functions into different well layers can be limited. A practical way to achieve such a goal is to grow a thin layer of AlSb in-between the InAs and GaSb well layers. The inserted AlSb layer can play a role as barrier for both electrons in the InAs layer and holes in the GaSb layer so that the electrons and holes are well separated in different well layers. Recently, the working InAs/AlSb/GaSb type II and broken-gap QWs have been successfully realized experimentally.[13] It is found that in an InAs/AlSb/GaSb QW with the layer widths, e.g., 17/1/5 nm, the effect of the hybridization of the electron and hole states is very weak. This is evident by the experiment that the electron and hole densities along with the electron and hole mobilities can be clearly measured through, respectively, the periodicities and the amplitudes of the Shubnikov–de Haas oscillations in Ref. 13. For InAs/AlSb/GaSb QWs with the layer widths around 17/1/5 nm in which the intentional doping is not introduced, the electron and hole densities are about 8×10^{11} cm^{-2} and 2×10^{11} cm^{-2}, respectively, and the electron and hole mobilities are about 9×10^{4} $\mathrm{cm}^{2}/\mathrm{V\,s}$ and 2×10^{4} $\mathrm{cm}^{2}/\mathrm{V\,s}$, respectively.[13] We also note that for such InAs/AlSb/GaSb QWs, the spin-splitting induced by the Rashba and Dressenhaus effects was not observed for magnetic field strength up to 9 T. These experimental findings indicate that in InAs/AlSb/GaSb QWs, the hybridization of the electron and hole states in different layers and the spin-splitting induced by inversion asymmetry of the microscopic confining potential can be greatly reduced.

The above mentioned experimental results suggest that InAs/AlSb/GaSb based type II and broken-gap QWs can be used as advanced electronic devices such as the HEMTs and HSFETs. Therefore, it is of great importance and significance to give a quantitative description on the influence of the inserted AlSb layer on electronic subband structure in InAs/AlSb/GaSb QWs. This becomes the prime motivation of the present theoretical study. In this paper, we develop a simple and straightforward eight-band $\mathbf{k}\cdot\mathbf{p}$ finite difference method (FDM) to calculate the electronic subband energy and wave function in InAs/AlSb/GaSb type II and broken-gap QWs, which is presented in Sec. II. In contrast to previous theoretical work,[9–12] the present study includes a thin AlSb layer inserted in-between the InAs and GaSb layers and we focus our attention on the effect of such AlSb layer on electronic subband structure in InAs/AlSb/GaSb QWs. The results obtained from this study are presented and discussed in Sec. III and the concluding remarks from the present investigation are summarized in Sec. IV.

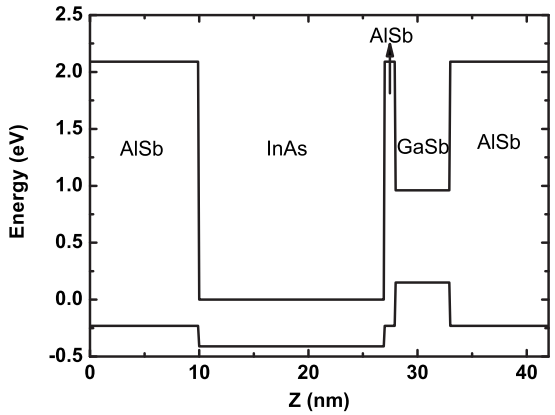

FIG. 1. Band alignment for an AlSb/InAs/AlSb/GaSb/AlSb type II and broken-gap QW.

II. THEORETICAL APPROACHES

In conjunction with the sample structures realized in recent experimental work,[13] here we consider an AlSb/InAs/AlSb/GaSb/AlSb QW structure in which a thin AlSb layer is inserted between the InAs and GaSb well layers, as shown in Fig. 1. When the thin AlSb layer is absent, the structure becomes a conventional InAs/GaSb type II and broken-gap QW. The growth direction is [001] which is defined as z axis. The x and y axes are along [100] and [010], respectively. In our model, the strain effect is neglected due to (i) the relatively small lattice mismatch among these materials, as pointed out by Ref. 5 and (ii) the presence of the inserted thin AlSb layer which can also reduce the strain at InAs/AlSb and GaSb/AlSb interfaces significantly. We start the calculation on electronic subband structure for such a QW system from an eight-band $\mathbf{k}\cdot\mathbf{p}$ model for the direct band gap and a zinc blende semiconductor. Two lowest conduction bands (CBs) and six highest valence bands [which are split into the heavy-hole (HH), light-hole (LH), and split-off hole bands at finite wave vector] are included. The contributions from remote bands such as split-off hole bands to the electron effective mass in the CB are included by following the approaches proposed by Fasolino and Altarelli.[14] The basic idea of the FDM is to use a layer or grid envelope function (i.e., F-basis) to construct the system Hamiltonian. Thus, one can describe, as accurately as possible, the most relevant portion of the electronic subband structures of a multilayer QW. The method developed here is transparent and can be

easily implemented. It is unnecessary to handle the complicated boundary conditions (BCs) like those used in the transfer matrix method. More importantly, the FDM can avoid the problem of numerical instability with respect to the transfer matrix method when the width of the QW become thick.

A. Kane Hamiltonian and envelope function approximation (EFA)

In the set of following Bloch basis functions:

$$u_1 = |s_{1/2,1/2}\rangle = |S\uparrow\rangle,$$

$$u_2 = |s_{1/2,-1/2}\rangle = |iS\downarrow\rangle,$$

$$u_3 = |p_{3/2,3/2}\rangle = -\frac{1}{\sqrt{2}}|(X+iY)\uparrow\rangle,$$

$$u_4 = |p_{3/2,1/2}\rangle = \frac{i}{\sqrt{6}}|(X+iY)\downarrow -2Z\uparrow\rangle,$$

$$u_5 = |p_{3/2,-1/2}\rangle = \frac{i}{\sqrt{6}}|(X+iY)\uparrow +2Z\downarrow\rangle,$$

$$u_6 = |p_{3/2,-3/2}\rangle = \frac{1}{\sqrt{2}}|(X-iY)\downarrow\rangle,$$

$$u_7 = |p_{1/2,1/2}\rangle = \frac{1}{\sqrt{3}}|(X+iY)\downarrow +Z\uparrow\rangle,$$

and

$$u_8 = |p_{1/2,-1/2}\rangle = \frac{i}{\sqrt{3}}|-(X-iY)\uparrow -Z\downarrow\rangle, \tag{1}$$

the 8×8 Kane Hamiltonian matrix can be written as

$$H_0(\mathbf{p}) = \begin{bmatrix} R & 0 & i\sqrt{3}S & \sqrt{2}T & iS^* & 0 & iT & \sqrt{2}S^* \\ 0 & R & 0 & iS & \sqrt{2}T & i\sqrt{3}S^* & \sqrt{2}S & iT \\ -i\sqrt{3}S^* & 0 & P+Q & iB & -G & 0 & -B/\sqrt{2} & i\sqrt{2}G \\ \sqrt{2}T & -iS^* & -iB^* & P-Q & 0 & G & -i\sqrt{2}Q & -\sqrt{3/2}B \\ -iS & \sqrt{2}T & -G^* & 0 & P-Q & -iB & -i\sqrt{3/2}B^* & -i\sqrt{2}Q \\ 0 & -i\sqrt{3}S & 0 & -G^* & iB^* & P+Q & i\sqrt{2}G^* & -B^*/\sqrt{2} \\ -iT & \sqrt{2}S^* & -B^*/\sqrt{2} & i\sqrt{2}Q & i\sqrt{3/2}B & -i\sqrt{2}G & P-\Delta & 0 \\ \sqrt{2}S & -iT & -i\sqrt{2}G^* & -\sqrt{3/2}B^* & i\sqrt{2}Q & -B/\sqrt{2} & 0 & P-\Delta \end{bmatrix}, \tag{2}$$

where

$$R = E_c + \left(\frac{1}{2m_c'}\right)(p_x^2+p_y^2+p_z^2),$$

$$P = E_v - \left(\frac{1}{2m_0}\right)\gamma_1(p_x^2+p_y^2+p_z^2),$$

$$Q = -\left(\frac{1}{2m_0}\right)\gamma_2(p_x^2+p_y^2-2p_z^2),$$

$$G = \left(\frac{1}{2m_0}\right)\sqrt{3}[\gamma_2(p_x^2-p_y^2) - 2i\gamma_3 p_x p_y],$$

$$B = \left(\frac{1}{2m_0}\right)2\sqrt{3}\gamma_3(p_x - ip_y)p_z,$$

$$T = \frac{1}{\sqrt{3}\hbar}P_0 p_z,$$

and

$$S = \frac{1}{\sqrt{6}\hbar}P_0(p_x + ip_y).$$

Here $\mathbf{p}=(p_x,p_y,p_z)$, $p_x=-i\hbar\partial/\partial x$ is the momentum operator along the x-direction, E_c and E_v are, respectively, the energy of CB and valence band edges, Δ is the spin split-off energy, m_0 is the free-electron mass, m_c' is the modified electron effective mass for the CB, γ_1, γ_2, and γ_3 are the modified Luttinger parameters for the valence band, and the interband matrix element is given by $P_0=-i(\hbar/m_0)\langle S|p_x|X\rangle$. The modified electron effective mass and the Luttinger parameters used in the band structure calculations are related by $1/m_c' = 1/m_e^* - 2E_p/3E_g - E_p/3(E_g+\Delta)$, $\gamma_1=\gamma_1^L - E_p/3E_g$, $\gamma_2=\gamma_2^L - E_p/6E_g$, and $\gamma_3=\gamma_3^L - E_p/6E_g$ with m_e^* being the true electron effective mass, E_g being the band gap, E_p being defined as $E_p=2m_0(P_0)^2/\hbar^2$, and γ_1^L, γ_1^L, γ_1^L being the true Luttinger parameters.

We take the usual expansion[15] of the wave function $\Psi_{\mathbf{k}_\parallel}(\mathbf{R})$ as a linear combination of zone center Bloch states $u_n(\mathbf{r})$ and $F_n(\mathbf{k}_\parallel,z)$, which reads

$$\Psi_{\mathbf{k}_\parallel}(\mathbf{r}) = \sum_{n=1}^{8} e^{i\mathbf{k}_\parallel \cdot \mathbf{r}} u_n(\mathbf{r}) F_n(\mathbf{k}_\parallel, z), \tag{3}$$

where $\mathbf{R}=(\mathbf{r},z)=(x,y,z)$, $\mathbf{k}_\parallel=(k_x,k_y)$ is the electron or hole wave vector along the 2D-plane, n is the band index, and $F(\mathbf{k}_\parallel,z)$ is the electron or hole wave function along the z-direction. Under the usual EFA, if $\Psi_{\mathbf{k}_\parallel}(\mathbf{R})$ is the solution of the multiband Schrödinger equation

$$[H_0(\mathbf{p}) + U(z) - E(\mathbf{k}_\parallel)]\Psi_{\mathbf{k}_\parallel}(\mathbf{R}) = 0, \tag{4}$$

$F_n(\mathbf{k}_\parallel,z)$ can be determined by solving

$$[H_0(\mathbf{k}_\parallel,p_z) + U(z) - E(\mathbf{k}_\parallel)]F(\mathbf{k}_\parallel,z) = 0, \tag{5}$$

where $U(z)$ is an external confining potential along the growth direction, which is mainly induced by the presence of the band offsets at the interfaces of different material layers. In the eight-band $\mathbf{k}\cdot\mathbf{p}$ approach, $F(\mathbf{k}_\parallel,z)$ may have eight components, each one multiplying the CB, HH band, LH band, and split-hole band basis states. The $\mathbf{k}\cdot\mathbf{p}$ Hamiltonian can be expanded into its polynomial form for p_z (the momentum operator along the z-direction) in the following way:

$$H_0(\mathbf{k}_\parallel,p_z) = H_0^{(2)}(\mathbf{k}_\parallel)p_z^2 + H_0^{(1)}(\mathbf{k}_\parallel)p_z + H_0^{(0)}(\mathbf{k}_\parallel), \tag{6}$$

where $H_0^{(j)}(\mathbf{k}_\parallel)$ for $j=0$, 1, and 2 were documented previously.[16,17] For future descriptions, we will write Eq. (6) in a more compact form as

$$\left[-H_0^{(2)}\frac{d^2}{dz^2} - iH_0^{(1)}\frac{d}{dz} + H_0^{(0)} + U(z)\right]F(z) = EF(z), \tag{7}$$

where $F(z)$ is a eight-component envelope function.

B. FDM

There are several methods to solve numerically the coupled ordinary differential equation given as Eq. (7), including the transfer matrix method,[18,19] the finite element method,[20] the basis expansion method,[21] etc. In this study, we employ the FDM to solve Eq. (5). Such approach is conceptually simple and easy to handle the BCs along with the ability to deal with arbitrary potentials. This method can also describe the tunneling effect with only a few changes and be with numerical stability in contrast to the transfer matrix method[18,19] which requires the truncation of growing exponential states. Following the FDM proposed previously,[22] we take the following discretization scheme

$$\begin{aligned} H_0^{(2)}\frac{\partial^2}{\partial z^2}F|_{z=z_l} &\to \frac{\partial}{\partial z}\left(H_0^{(2)}\frac{\partial}{\partial z}F\right)|_{z=z_l} \\ &\approx \frac{H_0^{(2)}(l+1)+H_0^{(2)}(l)}{2h^2}F_{l+1} \\ &\quad - \frac{H_0^{(2)}(l+1)+2H_0^{(2)}(l)+H_0^{(2)}(l-1)}{2h^2}F_l \\ &\quad + \frac{H_0^{(2)}(l-1)+H_0^{(2)}(l)}{2h^2}F_{l-1}, \end{aligned} \tag{8}$$

and

$$\begin{aligned} -iH_0^{(1)}\frac{\partial}{\partial z}F|_{z=z_l} &\to -\frac{i}{2}\left[H_0^{(1)}\frac{\partial}{\partial z}F + \frac{\partial}{\partial z}H_0^{(1)}F\right]|_{z=z_l} \approx \\ &\quad - i\frac{H_0^{(1)}(l+1)+H_0^{(1)}(l)}{4h}F_{l+1} \\ &\quad + i\frac{H_0^{(1)}(l-1)+H_0^{(1)}(l)}{4h}F_{l-1}. \end{aligned} \tag{9}$$

Here $F=F(\mathbf{k}_\parallel,z)$, $H_0^{(j)}=H_0^{(j)}(\mathbf{k}_\parallel)$, l labels the layer l along the growth direction of the QW (i.e., the z axis), and h is the step length between two adjacent layers. Now the application of the above scheme to Eq. (7) yields the following system of N algebraic equations (the multiband Schrödinger equation can be written in the layer F-basis)

$$H_{l,l-1}F_{l-1} + H_{l,l}F_l + H_{l,l+1}F_{l+1} = EF_l, \tag{10}$$

where $H_{l,l'}$ is the interaction between the layer l and the layer l', $E=E(\mathbf{k}_\parallel)$,

$$H_{l,l-1} = -\frac{H_0^{(2)}(l-1)+H_0^{(2)}(l)}{2h^2} + i\frac{H_0^{(1)}(l-1)+H_0^{(1)}(l)}{4h},$$

$$H_{l,l} = \frac{H_0^{(2)}(l+1)+2H_0^{(2)}+H_0^{(2)}(l-1)}{2h^2} + H_0^{(0)} + U(l),$$

and

$$H_{l,l+1} = -\frac{H_0^{(2)}(l+1)+H_0^{(2)}(l)}{2h^2} - i\frac{H_0^{(1)}(l+1)+H_0^{(1)}(l)}{4h}. \tag{11}$$

These equations are derived from the discretized 8×8 Hamiltonian matrices and they are valid for the interactions between two adjacent layers located both in the same material and in the two different materials. Namely, they hold for the interactions across the sample structure. The eigenproblem Eq. (9) can be written in a matrix form to better appreciate its sparse structure

$$\begin{bmatrix} H_{11} & H_{12} & 0 & \cdots & \cdots & \cdots & H_{10}^* \\ H_{21} & H_{22} & H_{23} & 0 & \cdots & \cdots & 0 \\ 0 & H_{32} & H_{33} & H_{34} & 0 & \cdots & 0 \\ \vdots & \vdots & \vdots & \vdots & \vdots & \vdots & \vdots \\ 0 & \cdots & \cdots & 0 & H_{N-1N-2} & H_{N-1N-1} & H_{N-1N} \\ H_{NN+1}^* & 0 & \cdots & \cdots & 0 & H_{NN-1} & H_{NN} \end{bmatrix} \times \begin{bmatrix} F_1 \\ F_2 \\ \vdots \\ \vdots \\ F_{N-1} \\ F_N \end{bmatrix} = E\begin{bmatrix} F_1 \\ F_2 \\ \vdots \\ \vdots \\ F_{N-1} \\ F_N \end{bmatrix}, \tag{12}$$

where H_{10}^* and H_{NN+1}^* express the BCs. When studying a QW, the BCs are that the wave function must vanish far from the well region. This is accomplished by setting the barrier region wide enough and requesting $F_0=F_{N+1}=0$, which translates into $H_{10}^*=H_{NN+1}^*=0$. When investigating a superlattice

TABLE I. Band parameters for bulk AlSb, InAs, and GaSb taken from Ref. 5. Here, m_e^* is the electron effective mass without including the contributions from the remote bands and γ_1^L, γ_1^L, γ_1^L are the true Luttinger parameters.

Parameter	AlSb	InAs	GaSb
E_g (eV)	2.32	0.41	0.81
E_p (eV)	18.7	22.2	22.4
Δ_{so} (eV)	0.75	0.38	0.75
m_e^*/m_0	0.18	0.023	0.042
γ_1^L	4.15	19.67	11.80
γ_2^L	1.01	8.37	4.03
γ_3^L	1.75	9.26	5.26

(SL) problem, the Bloch BCs apply, which request that $F_{N+1}=e^{iqd}F_1$ and $F_0=e^{-iqd}F_N$ translating into $H^*_{NN+1}=e^{iqd}H_{NN+1}$ and $H^*_{10}=e^{-iqd}H_{10}$ with q and d being, respectively, the SL periodicity and wave vector along z-direction. Thus, after obtaining the discretized Hamiltonian matrix in Eq. (12), we are able to calculate the electronic subband structure by using the standard subroutines available in the LINPACK mathematical subroutine libraries[23] to diagonalize the discretized Hamiltonian matrices.

III. NUMERICAL RESULTS AND DISCUSSIONS

In this paper, we calculate the energy spectra and the electron and hole wave functions in AlSb/InAs/GaSb/AlSb and AlSb/InAs/AlSb/GaSb/AlSb QWs. The CB and valence band parameters for bulk AlSb, InAs, GaSb are listed in Table I. The bottom of the CB in the InAs layer is taken as the zero energy reference. The valence band offsets are 0.56 eV for GaSb/InAs heterojunction, 0.18 eV for AlSb/InAs heterojunction, and −0.38 eV for AlSb/GaSb heterojunction. Here we do not consider the effect of charge transfer in different layers, which requires a self-consistent calculation of coupled Schrödinger and Poisson equations and complicates the analytical and numerical calculations considerably. Furthermore, in the present study, the strain effect is not taken into account due to the small lattice mismatch among InAs, GaSb and AlSb layers, as pointed out by Ref. 5 and the presence of the inserted thin AlSb layer which can reduce the strain at InAs/AlSb and GaSb/AlSb interfaces significantly. For the given InAs/AlSb/GaSb layer widths in an AlSb/InAs/AlSb/GaSb/AlSb QW, we are able to calculate the energy spectrum $E(\mathbf{k}_\parallel)$ and the normalized probability density $|\Psi(z)|^2=\Sigma_{n=1}^{8}|F_n(\mathbf{k}_\parallel,z)|^2$ at the zone center ($\mathbf{k}_\parallel=0$) and finite wave vector $\mathbf{k}_\parallel$. In conjunction with sample devices used in the experimental investigation,[13] our numerical calculations are performed mainly for an InAs/AlSb/GaSb QW in which the InAs/AlSb/GaSb well widths are $17/d/5$ nm with d being the inserted AlSb layer thickness.

A. AlSb/InAs/GaSb/AlSb QWs

We first consider the case of an InAs/GaSb QW with $d=0$. Figure 2 shows the dispersion relation of the electronic subbands in an AlSb/InAs/GaSb/AlSb QW with a 17 nm InAs layer and a 5 nm GaSb layer. The results are shown for the "spin-up" (solid curves) and "spin-down" (dashed curves) electron and hole states in the absence of the inserted

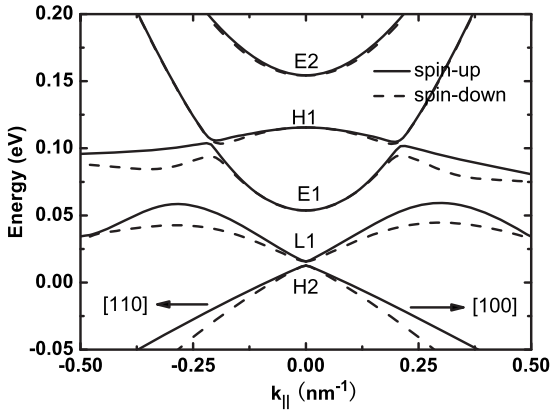

FIG. 2. The energy spectrum, $E(\mathbf{k}_\parallel)$, for electrons and holes in an AlSb/InAs/GaSb/AlSb QW as a function of the wave vector $k_\parallel$ at the fixed InAs/GaSb layer widths 17/5 nm. The solid and dashed curves are for spin-up and spin-down states.

AlSb layer between the InAs and GaSb layers. There are five subbands of interest, which are labeled as $E1$ and $E2$ for, respectively, the ground and first-excited electron subbands, $H1$ and $H2$ for, respectively, the first and second HH subbands, and $L1$ for the ground light-hole (LH) subband. The assignment of carrier type to various subbands follows the associated wave function properties at $\mathbf{k}_\parallel=0$.[9] The defined electron states are mainly confined in the InAs layer and the hole states are mainly confined in the GaSb layer. As can be seen from Fig. 2, the bottom of the $E1$ subband is well below the top of the $H1$ subband, which confirms that when the InAs/GaSb layer widths are about 17/5 nm, the broken-gap structure can be achieved in an InAs/GaSb QW. We find that there is only a weak coupling between the $E1$ subband and the $H1$ subband when $\mathbf{k}_\parallel=0$. At $\mathbf{k}_\parallel=0$, the spin-up and spin-down states in each subband are degenerate. This implies that the zero-field spin-splitting does not occur at $\mathbf{k}_\parallel=0$ in an InAs/GaSb QW. The strength of the coupling between the $E1$ and $H1$ subbands increases markedly with increasing the value of $|\mathbf{k}_\parallel|$, leading to an anticrossing phenomenon and to a hybridization gap of about 10 meV at the point of $|\mathbf{k}_\parallel|=0.21$ nm^{-1}. Due to the presence of the spin-orbit interaction in such an asymmetric QW structure, each subband is split into the usual spin-up and spin-down branches at zero magnetic field. Thus, two hybridization gaps are induced by different spin states at the anticrossing points and the position as well as magnitude of the gap are spin-dependent. Moreover, over the whole regime of $\mathbf{k}_\parallel$ the coupling between the $E1$ subband and the $L1$ subband is very weak because the $E1$ subband is well above the $L1$ level.

The band hybridization phenomenon in the interested QW shown in Fig. 2 can be demonstrated more clearly by looking into the features of the probability density $|\psi(z)|^2=|F_n(\mathbf{k}_\parallel,z)|^2$ for the spin-up and spin-down states. We know that in such a QW structure, the electrons and holes are located mainly within the InAs and GaSb layers, respectively. Therefore, checking the probability density of a wave function can help to determine the features of the corresponding electronic state, i.e., the electronlike or holelike of the hybridized states. The results for $|\psi(z)|^2$ at $\mathbf{k}_\parallel=0$ and finite $\mathbf{k}_\parallel$ are presented, respectively, in Figs. 3 and 4 for the same

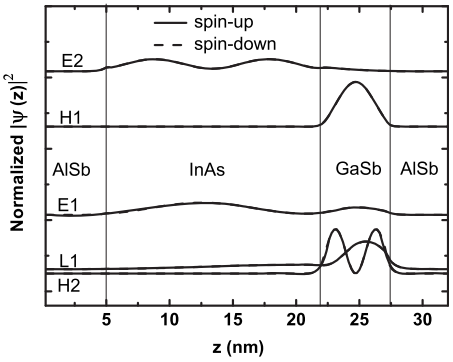

FIG. 3. Normalized probability distribution for different subbands at the zone center $k_{\|}=0$ for the same sample parameters as in Fig. 2. Here the normal thinner lines are the interfaces between different material layers as indicated and the curves for the spin-up and spin-down states coincide.

sample structure as in Fig. 2. Here each probability density is normalized to unity and the curves are shifted and ordered according to their corresponding subband energies at the zone center. From Fig. 3, one can see clearly that the $E1$ and $E2$ states are confined mainly within the InAs layer, whereas the $H1$, $H2$, and $L1$ states are confined mainly within the GaSb layer. This is due to the fact that at $\mathbf{k}_{\|}=0$, the coupling among different subbands is very weak (as also shown in Fig. 2). Consequently, when the InAs/GaSb layer widths are about 17/5 nm the broken-gap and type II structure can be achieved in the proposed QW at $\mathbf{k}_{\|}=0$. Because the spin-up and the spin-down states are degenerate at $\mathbf{k}_{\|}=0$ (as shown in Fig. 2), the probability densities for different spin states in a certain subband are exactly the same in Fig. 3. At a finite wave vector $\mathbf{k}_{\|}$, the spin degeneracy is lift and the band mixing and hybridization occur. As shown in Fig. 4, the difference of probability density for the spin-up and spin-down states in a certain subband can be markedly observed when $|\mathbf{k}_{\|}|=0.21$ nm^{-1} at which the band anticrossing takes place (see Fig. 2). At $|\mathbf{k}_{\|}|=0.21$ nm^{-1}, the $E1$ and $H1$ states are strongly coupled so that a major part of the $E1$ states is located within the GaSb layer and a considerable part of the $H1$ states is located within the InAs layer. In such a case, the hybridized $E1-H1$ states are formed in the QW. This feature is in sharp contrast to the case of $\mathbf{k}_{\|}=0$ shown in Fig. 3. Due to a relatively weak coupling between the $L1$ subband and other subbands, the $L1$ states are still confined mainly within the GaSb layer. From Fig. 4, we also find that the coupling

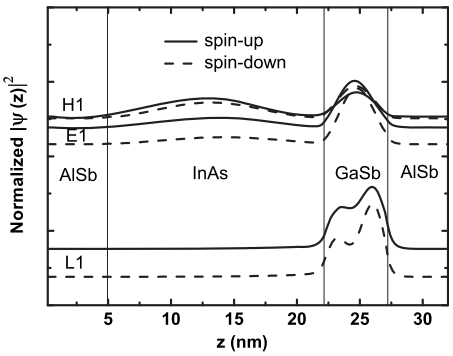

FIG. 4. Normalized probability distribution for the $E1$, $H1$, and $L1$ subbands at $|\mathbf{k}_{\|}|=0.21$ nm^{-1} for the same sample parameters as in Fig. 2.

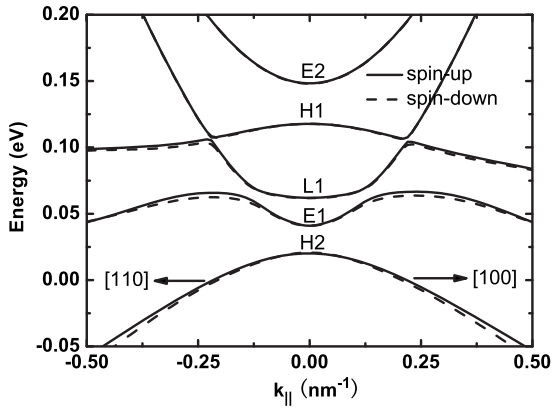

FIG. 5. Energy spectra for the $E1$, $E2$, $H1$, $H2$, and $L1$ subbands in an AlSb/InAs/AlSb/GaSb/AlSb QW with the InAs/AlSb/GaSb layer widths 17/1/5 nm. The results are shown for different spin states.

between the spin-down $E1$ states and the spin-down $H1$ states is stronger than that between the spin-up $E1$ states and the spin-up $H1$ states. This results in a larger hybridization gap for the spin-down states than for the spin-down states at the anticrossing points as observed in Fig. 2.

B. AlSb/InAs/AlSb/GaSb/AlSb QWs

From now on we consider the case of InAs/AlSb/GaSb QWs with finite d, in conjunction with the sample devices used in experimental work.[13] We present and discuss the features of the electronic subband structure in AlSb/InAs/AlSb/GaSb/AlSb QW structures (see Fig. 1). The electronic energy spectra for the $E1$, $E2$, $H1$, $H2$, and $L1$ subbands are shown in Fig. 5 for an InAs/AlSb/GaSb QW with layer widths 17/1/5 nm, where a thin AlSb layer is inserted between the InA and GaSb layers. Comparing Fig. 5 with those shown in Fig. 2, we note that in the presence of the inserted AlSb layer, (i) the band hybridization between the $E1$ and $H1$ subbands observed in Fig. 2 does not occur because the $H1$ states is now too much higher than the $E1$ states over the whole $\mathbf{k}_{\|}$ regime; (ii) the bottom of the $L1$ subband is now well above the bottom of the $E1$ subband and, as a result, the band hybridization and mixing between the $E1$ and $L1$ subbands can be observed at finite $\mathbf{k}_{\|}$. The anticrossing points for such $E1-L1$ hybridization are found to be around $|\mathbf{k}_{\|}|=0.15$ nm^{-1}; (iii) the hybridization between the $H1$ and $L1$ subbands can be observed clearly and the corresponding anticrossing phenomenon occurs still at about $|\mathbf{k}_{\|}|=0.21$ nm^{-1}. This is in contrast to those shown in Fig. 2 where the anticrossing phenomenon occurs at $|\mathbf{k}_{\|}|=0.21$ nm^{-1} but for $E1$ and $H1$ subbands; (iv) at the anticrossing points $|\mathbf{k}_{\|}|=0.21$ nm^{-1} the coupling between the $L1$ states and the $H1$ states is relatively weak and, consequently, the hybridization gap reduces to about 4 meV in contrast to a 10 meV gap shown in Fig. 2. On the other hand, the coupling between the $E1$ and $L1$ states is quite strong at the anticrossing points $|\mathbf{k}_{\|}|=0.14$ nm^{-1} where the hybridization gap is about 11 meV; and (v) the strength of the spin-splitting in all these subbands decreases significantly due to the presence of the inserted AlSb layer which reduces the structural inversion asymmetry in the InAs/AlSb/GaSb QW, compared with the

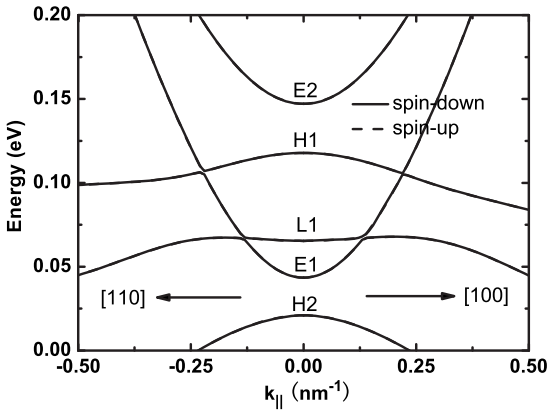

FIG. 6. Energy spectra for the $E1$, $E2$, $H1$, $H2$, and $L1$ subbands in an AlSb/InAs/AlSb/GaSb/AlSb QW with the InAs/AlSb/GaSb layer widths 17/3/5 nm. The results are shown for different spin states.

conventional InAs/GaSb QW. In Fig. 6, we demonstrate that when the inserted AlSb layer thickness is $d=3$ nm, the band hybridization and spin-splitting are almost fully reduced.

The influence of the inserted AlSb layer on electronic subband structure in the InAs/AlSb/GaSb QWs can be examined again by looking into the features of the normalized probability densities for different subbands at the zone center and finite wave vector $\mathbf{k}_\parallel$. In Fig. 7, $|\Psi(z)|^2$ for different subbands at the zone center $\mathbf{k}_\parallel=0$ are shown as a function of the distance along the growth direction. We see again that at $\mathbf{k}_\parallel=0$ the electrons/holes are mainly located within the InAs/GaSb layers and the zero-field spin-splitting is not observable, similar to those shown in Fig. 3 for an InAs/GaSb QW. In Fig. 8 $|\psi(z)|^2$ for different subbands at anticrossing point $|\mathbf{k}_\parallel|=0.21$ nm^{-1} are shown as a function of the distance along the growth direction. As shown in Fig. 5, at $|\mathbf{k}_\parallel|=0.21$ nm^{-1}, the hybridization gap at the anticrossing points between the $H1$ and $L1$ states can be observed. At this point of $\mathbf{k}_\parallel$, it is the $H1$ subband and the $L1$ subband not the $H1$ subband and the $E1$ subband as shown in Fig. 4 are hybridized. Furthermore, due to the presence of the interactions among different subbands, the spin-splitting can be observed clearly although the strength of the spin-splitting is relatively weaker comparing with those shown in Fig. 4 for an InAs/GaSb QW. In Fig. 9, we plot the normalized probability densities for different subbands as a function of the distance of the growth direction at anticrossing point $|\mathbf{k}_\parallel|=0.14$ nm^{-1}. From Fig. 5, we know that at anticrossing point $|\mathbf{k}_\parallel|=0.14$ nm^{-1}, the hybridization gap between $E1$ and $L1$ states can be seen. Because the $E1$ and $L1$ subbands are now hybridized, a major part of electron distribution for the $E1$ subband is in the GaSb layer whereas a significant part of LH distribution is in the InAs layer. These results indicate that due to the $E1-L1$ hybridization the $L1$ states become electronlike while the $E1$ states turn into LH-like. This phenomenon was also observed and documented by other authors for InAs/GaSb QW structures with thick GaSb layer widths.[9] Because the hybridization gap between the $E1$ and $L1$ subbands can be observed at relatively smaller $\mathbf{k}_\parallel$, the spin-splitting at $|\mathbf{k}_\parallel|=0.14$ nm^{-1} shown in Fig. 9 is found to be much smaller than that at $|\mathbf{k}_\parallel|=0.21$ nm^{-1} shown in Fig. 8 for $H1$ and $L1$ hybridization. It should be noted that the $E1$ and $L1$ states have relatively small effective electron masses. Thus, the stronger interactions between the $E1$ and $L1$ subbands can be expected and, hence, the hybridization gap between the $E1$ and $L1$ subbands is much larger than that induced by hybridization between the $L1$ and $H1$ states.

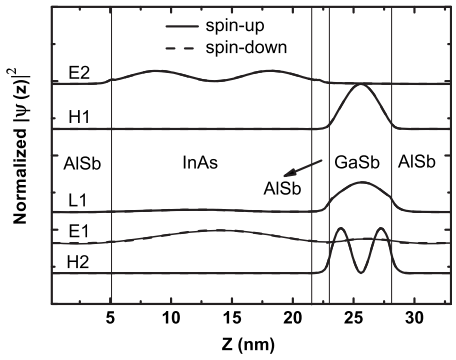

FIG. 7. Distribution of the normalized probability density at the zone center $\mathbf{k}_\parallel=0$ for a QW with the same sample parameters as in Fig. 5. The normal thinner lines are the interfaces between different material layers as indicated and the curves for the spin-up and spin-down states coincide.

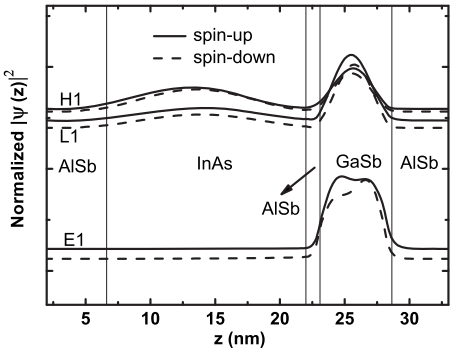

FIG. 8. Distribution of the normalized probability density at $|\mathbf{k}_\parallel|=0.21$ nm^{-1} for a QW with the same sample parameters as in Fig. 5.

The dependence of the hybridization gaps, induced by the coupling between the $E1$ and $H1$ subbands at $|\mathbf{k}_\parallel|=0.21$ nm^{-1} (Δ_1 and Δ_2) and between the $E1$ and $L1$ subbands at $|\mathbf{k}_\parallel|=0.15$ nm^{-1} (Δ_3 and Δ_4), on the width of the inserted AlSb layer in InAs/AlSb/GaSb QWs is shown in Fig. 10 for different spin states. We notice that: (i) the hybridization gaps decrease quickly with increasing the width of the inserted AlSb layer. This indicates that the AlSb layer

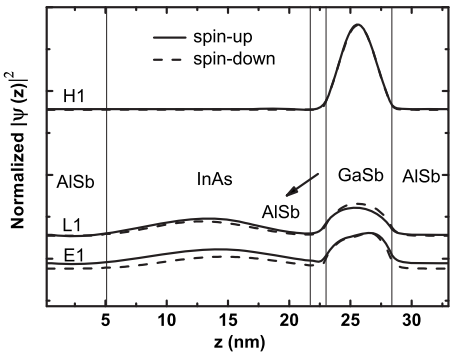

FIG. 9. Distribution of the normalized probability density at $|\mathbf{k}_\parallel|=0.14$ nm^{-1} for a QW with the same sample parameters as in Fig. 5.

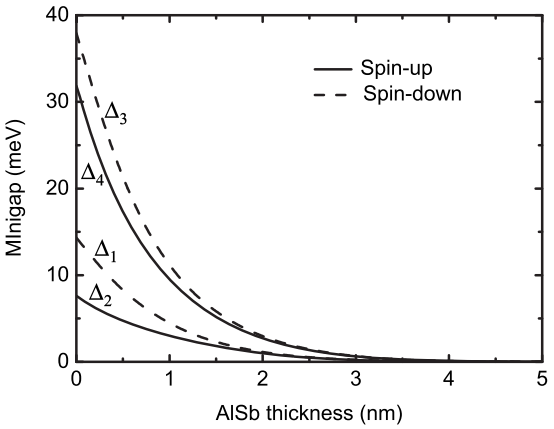

FIG. 10. Energy of the hybridization gaps as a function of the inserted AlSb layer thickness for AlSb/InAs/AlSb/GaSb/AlSb QWs with a 17 nm InAs layer and a 5 nm GaSb layer. The energy gaps are measured for different spin states at the anticrossing points $|\mathbf{k}_{\|}|=0.21$ nm^{-1} for the $E1$ and $H1$ hybridization (Δ_1 and Δ_2) and at $|\mathbf{k}_{\|}|=0.14$ nm^{-1} for the $E1$ and $L1$ hybridization (Δ_3 and Δ_4).

placed in-between the InAs/GaSb layers can indeed reduce the band hybridization in the InAs/AlSb/GaSb QWs; (ii) the hybridization gaps induced by coupling within the spin-up states (Δ_2 and Δ_4) are smaller than those caused by interactions within the spin-down states (Δ_1 and Δ_3); (iii) the difference of the hybridization gaps induced by different spin states decreases rapidly with increasing the AlSb layer width. This confirms further that the inserted AlSb layer can reduce the zero-field spin-splitting in the InAs/AlSb/GaSb QW structures; and (iv) when the AlSb layer thickness is larger than 3 nm, the hybridization gaps for $E1$ and $H1$ coupling and for $E1$ and $L1$ coupling close to zero and the differences between Δ_1 and Δ_2 and between Δ_3 and Δ_4 can be neglected. It should be noted that the inserted AlSb layer in an InAs/AlSb/GaSb QW serves mainly as a barrier with a large barrier height for both electrons and holes. Thus, the AlSb layer can suppress the tunneling of electrons (holes) from the InAs (GaSb) layer to the GaSb (InAs) layer and can reduce the kinetic interactions among different subbands in different material layers. As a result, the band hybridization and spin-splitting in the device system can be reduced significantly in the presence of the AlSb layer.

C. Further remarks

The results shown and discussed above demonstrate that the presence of the thin AlSb layer in an InAs/AlSb/GaSb type II and broken-gap QW can alter the features of the electronic subband structure dramatically, in comparison with the conventional InAs/GaSb QWs. The most important and interesting feature for an InAs/AlSb/GaSb type II and broken-gap QW with the layer widths 17/1/5 nm is that the $L1$ states are hybridized with both $E1$ and $H1$ subbands whereas the $E1$ subband does not mix at all with the $H1$ subband. The hybridization between the $E1$ and $H1$ subbands can be observed in a conventional InAs/GaSb QW and such hybridization can lower the mobilities of the carriers.[8] For typical InAs/AlSb/GaSb type II and broken-gap QWs (Ref. 13) with electron density about 8×10^{11} cm^{-2}, the Fermi level is well above the bottoms of the $E1$ and $L1$ subbands and is below the top of the $H1$ subband in Fig. 5. This implies that in such structure the $E1$ subband is populated by electrons and the $H1$ subband is occupied by HHs. Although the $L1$ subband is hybridized with both $E1$ and $H1$ subbands, the $L1$ subband is not populated with LHs. Thus, in an InAs/AlSb/GaSb QW the conducting carriers are still electrons in the InAs layer and HHs in the GaSb layer similar to an InAs/GaSb QW. However, the $E1$ subband is hybridized with the $H1$ subband in a conventional InAs/GaSb QW whereas there is no mixing and hybridization between $E1$ and $H1$ subband in an InAs/AlSb/GaSb QW. This is the main reason why experimentally the electrons and holes can well be identified and why the larger electron and hole mobilities can be measured in InAs/AlSb/GaSb QWs. The suppression of the band hybridization between $E1$ and $H1$ subbands and of the spin-splitting in the device can reduce significantly the electron-hole coupling via Coulomb interaction in an InAs/AlSb/GaSb QW. This can further enlarge the carrier mobilities in the QW structure. Moreover, the reduction in the electron–hole interaction in the sample structure implies that in an InAs/AlSb/GaSb type II and broken-gap QW the type II excitonic effect can be neglected in analyzing the experimental results[13] and in the theoretical modeling.[24]

IV. CONCLUSIONS

In this work we have developed a simple and straightforward eight-band $\mathbf{k}\cdot\mathbf{p}$ FDM to calculate the electronic subband structure in conventional AlSb/InAs/GaSb/AlSb based and in AlSb/InAs/AlSb/GaSb/AlSb based type II and broken-gap QW structures. We have examined the influence of the inserted AlSb layer on band hybridization and spin-splitting in AlSb/InAs/AlSb/GaSb/AlSb QWs. Our results demonstrate that the electronic subband structure in an InAs/AlSb/GaSb QW, especially the features of the band hybridization and spin-splitting, differs sharply from that in a conventional InAs/GaSb QW. On the basis of the obtained theoretical results, we are able to explain why in InAs/AlSb/GaSb based type II and broken-gap QWs the conducting electrons and holes can be well identified and high electron and hole mobilities can be achieved experimentally. We hope the results obtained from the present theoretical study and from our recent experimental work can shed some lights on the investigation and application of AlSb/InAs/AlSb/GaSb/AlSb QW systems as advanced electronic and optoelectronic devices.

ACKNOWLEDGMENTS

This work was supported by the Chinese Academy of Sciences (Grant No. 2007CB925004), National Natural Science Foundation of China (Grant No. 90503005), and by the Department of Science and Technology of Yunnan Provence.

[1]H. Munekata, J. C. Maan, L. L. Chang, and L. Esaki, J. Vac. Sci. Technol. B **5**, 809 (1987).
[2]M. Altarelli, Phys. Rev. B **28**, 842 (1983).
[3]I. Lo, W. C. Mitchel, R. Kaspi, S. Elhamri, and R. S. Newrock, Appl. Phys. Lett. **65**, 1024 (1994).
[4]J.-P. Cheng, J. Kono, B. D. McCombe, I. Lo, W. C. Mitchel, and C. E. Stutz, Phys. Rev. Lett. **74**, 450 (1995).
[5]E. Halvorsen, Y. Galperin, and K. A. Chao, Phys. Rev. B **61**, 16743

(2000).
[6]R. Beresford, L. F. Luo, K. F. Longenbach, and W. I. Wang, Appl. Phys. Lett. **56**, 952 (1990).
[7]H. J. Haugan, F. Szmulowicz, G. J. Brown, and K. Mahalingam, J. Appl. Phys. **96**, 2580 (2004).
[8]M. Lakrimi, S. Khym, R. J. Nicholas, D. M. Symons, F. M. Peeters, N. J. Mason, and P. J. Walker, Phys. Rev. Lett. **79**, 3034 (1997).
[9]A. Zakharova, S. T. Yen, and K. A. Chao, Phys. Rev. B **64**, 235332 (2001).
[10]R. Magri, L. W. Wang, A. Zunger, I. Vurgaftman, and J. R. Meyer, Phys. Rev. B **61**, 10235 (2000).
[11]X. Cartoixà, D. Z.-Y. Ting and T. C. McGill, Phys. Rev. B **68**, 235319 (2003).
[12]S. de-Leon, L. D. Shvartsman, and B. Laikhtman, Phys. Rev. B **60**, 1861 (1999).
[13]P. A. Folkes, G. Gumbs, W. Xu, and M. T. Lara, Appl. Phys. Lett. **89**, 202113 (2006).
[14]A. Fasolino and M. Altarelli, Surf. Sci. **142**, 322 (1984).
[15]G. Bastard, Phys. Rev. B **24**, 5693 (1981).
[16]D. L. Smith and C. Mailhiot, Phys. Rev. B **33**, 8345 (1986).
[17]F. Szmulowicz, Phys. Rev. B **54**, 11539 (1996).
[18]L. R. Ram-Mohan, K. H. Yoo, and R. L. Aggarwal, Phys. Rev. B **38**, 6151 (1988).
[19]S. L. Chuang, Phys. Rev. B **43**, 9649 (1991).
[20]K. Nakamura, A. Shimizu, M. Koshiba, and K. Hayata, IEEE J. Quantum Electron. **27**, 2053 (1991).
[21]G. E. W. Bauer and T. Ando, Phys. Rev. B **38**, 6015 (1988).
[22]S. L. Chuang and C. S. Chang, Semicond. Sci. Technol. **12**, 252 (1997).
[23]J. J. Dongarra, J. R. Bunch, G. B. Moler, and G. W. Stewart, *LINPACK User Guide* (Society for Industries and Applied Mathematics, Philadelphia, 1979).
[24]W. Xu, P. A. Folkes, and G. Gumbs, J. Appl. Phys. **102**, 033703 (2007).